Multi-Displacement Microstructure Modeling of Two-Dimensional Elastic Metamaterials

A.P.Liu[a,b], G.K. Hu[a], Z. H. Jin[c] and G.L.Huang[b,*]
a School of Aerospace Engineering, Beijing Institute of Technology, Beijing, 100081, China
b Department of Systems Engineering, University of Arkansas at Little Rock, AR, 72204, USA
c Department of Mechanical Engineering, University of Maine, ME, 04469, USA
E-mail Address: glhuang@ualr.edu

ABSTRACT

In this paper, an elastic metamaterial made of lead cylinders coated with elliptical rubbers in an epoxy matrix is considered, and a new multi-displacement microstructure model is proposed to capture the dipolar resonant motion. In the formulation, additional displacement and kinematic variables are introduced to describe global and local deformations, respectively. For the chiral metamaterial, one more rotation variable is needed. The macroscopic governing equations of the two-dimensional elastic metamaterial are explicitly derived. To verify the multi-displacement model, the wave dispersion curves from the current model are compared with those from the finite element simulation for wave propagation. The good agreement is observed in both the longitudinal and transverse wave modes.

Keywords: Elastic Metamaterial, Multi-displacement, Microstructure, Wave propagation

1. INTRODUCTION

Metamaterials are a new class of ordered composites that exhibit exceptional electromagnetic, optic and mechanical properties not readily observed in nature [1, 2]. Although electromagnetic (EM) and acoustic metamaterials have been studied intensively, elastic metamaterials have received much less attention, despite the fact that elastic metamaterials offer richer behaviors as they enable both longitudinal and transverse waves to propagate. Various novel concepts and engineering applications of elastic metamaterials have been successfully demonstrated such as mechanical filters, sound and vibration isolators, elastic waveguides and energy harvesting [3-8].

To understand global wave mechanism in elastic metamaterials, the most important and efficient approach is homogenization. For isotropic elastic metamaterials, conventional homogenization will result in three independent effective parameters: effective mass density, effective bulk modulus and effective shear modulus. Until now, several homogenization methods have been developed to model this kind of materials as effective homogeneous elastic media. Those methods include the plane wave expansion (PWE) technique, the coherent potential approximation (CPA), the micromechanics analytical model or multiple scattering theory (MST) based on the long-wavelength limit [9-16]. By requiring only the wavelength in the matrix to be much larger than the size of the microstructures, the extension of the CPA or effective medium theory (EMT) was further developed to predict the effective properties of the elastic metamaterials [17]. However, these analytical methods are mainly based on the analytical scattering solution of

Health Monitoring of Structural and Biological Systems 2012, edited by Tribikram Kundu, Proc. of SPIE Vol. 8348, 834825 · © 2012 SPIE · CCC code: 0277-786X/12/$18 · doi: 10.1117/12.915039

microstructures with simple geometries (sphere or cylinder). To achieve the desirable effective properties, elastic metamaterials with complex microstructures or microstructure arrangements must be designed. For nonelementary microstructure geometries, an exact analytical model is not practicable and computational techniques should be suggested such as the multiple multipole (MMP) method [18], lumped mass method [19], and finite difference method [20]. For the acoustic metamaterial, the anisotropic effective mass density can be achieved by changing position or distribution array of the microstructure in the unit cell [21, 22]. However, for the elastic metamaterial, the microstructure geometry should be properly designed to obtain the anisotropic effective mass density [23-26]. A 2D elastic resonator of arbitrary geometry was systematically studied through a finite element modal analysis [27]. Gu et al. [28] investigated local resonance modes of elliptic cylinders coated with silicon rubber in a rigid matrix to obtain the anisotropic effective mass density. However, most of these methods mainly focus on understanding of local resonant mechanism. Practically, one may want to predict dynamic behavior of the elastic metamaterial by using an effective continuum model, wherein effects of the microstructure are included in effective properties and/or in macro-dynamics equations. The obtained macro-dynamics equations can be applied to problems of time-dependent vibration and transit wave propagation in the finite and infinite structures, which is important for potential engineering applications of metamaterial devices. However, continuum homogenization of elastic metamaterials with complex microstructures is a challenging task.

Until now, few efforts have been made to study the effective properties beyond the quasi-static limit or in higher frequency regions, although some interesting wave phenomena occur only when the wavelength is comparable to the lattice scale. To describe wave propagation problems with wavelengths in an order of dimensions of microstructures, Wozniak [29] proposed a non-asymptotic approach of macro-dynamics modeling of composite. Milton and Willis [30] and Milton [31] presented a rigorous theoretical foundation for the dynamic effective parameters of the elastic metamaterial beyond the quasi-static limit. The microscale effects due to non-local behavior were explained by the modification of linear continuum elastodynamic equations. Similar efforts have been made through work on metamaterials with a macroscopic higher order gradient or non-local elastic response [32]. An alternative approach is to employ additional kinematic variables to describe the nonhomogeneous local deformation in the microstructure of the solid. This approach leads to Cosserat continuum models [33, 34] or micropolar models [35, 36] or strain gradient theory [37] or the microstructure continuum theory [38, 39]. Microstructure continuum theory has recently been adopted to describe global dynamic behavior of isotropic elastic metamaterials with discrete microstructures (a mass-spring system) [40] and of anisotropic elastic metamaterials with continuous media [41]. Accuracy of the model was verified by comparison with the results obtained from the finite element method. However, the microstructure continuum model or high-order continuum model has a difficulty to capture the dipolar motion, in which the inner inclusion moves out of phase with respect to motion of the matrix in elastic metamaterials. Additional displacement variables are needed to capture the dipolar motion.

In this paper, an elastic metamaterial made of lead cylinders coated with elliptical rubbers in an epoxy matrix is considered. To analytically obtain global governing equations of motion in the elastic metamaterial, the complex continuous microstructure is simplified to a discrete mass-spring system based on strain energy equivalence. Based on the simplified system, a new multi-displacement microstructure theory is developed to capture both dipolar local resonant motion and microstructure deformation by introducing both multi-displacement variables and micro-deformation variables, which are not considered in the conventional continuum model. For the chiral metamaterial,

one more rotation variable is needed. The macroscopic governing equations of the two-dimensional elastic metamaterial are explicitly derived. To verify the multi-displacement model, the wave dispersion curves from the current model are compared with those from the finite element simulation for wave propagation. The good agreement is observed in both the longitudinal and transverse wave modes.

2. A multi-displacement microstructure model for 2D metamaterial

In this study, an anisotropic elastic metamaterial made of heavy cylinder cores coated with elliptical soft layer and embedded in a matrix is considered, as shown in Fig. 1(a), and its representative volume element (RVE) is identified in Fig. 1(b). The microstructure is distributed in a rectangular lattice array. In the figure, the hard inclusion core is labeled as medium 1, the soft coating medium is labeled as medium 2, and the matrix is labeled as medium 3. The isotropic material constants of the inclusion core, the coating layer and the matrix are ρ_1, E_1, ν_1; ρ_2, E_2, ν_2 and ρ_3, E_3, ν_3, respectively. The radius of the core is a. The lattice constants along the X_2 and X_3 directions are denoted as d_2 and d_3. The semimajor and semiminor axes of the ellipse are denoted as $b_1$and b_2, respectively. In the unit cell (k,l), position of the center point is given in the global coordinate $X_2 = {X_2}^l$ and $X_3 = {X_3}^k$. For convenience, we define a local polar coordinate system (r,θ) as well as a local Cartesian coordinates (x_2,x_3)in the unit cell with $x_2 = rcos\theta$ and $x_3 = rsin\theta$, as shown in Fig. 1(b). Strong anisotropic properties of the metamaterial along the X_2 and X_3 directions can be achieved by adjusting dimensions of the major and minor axes of the coating ellipse.

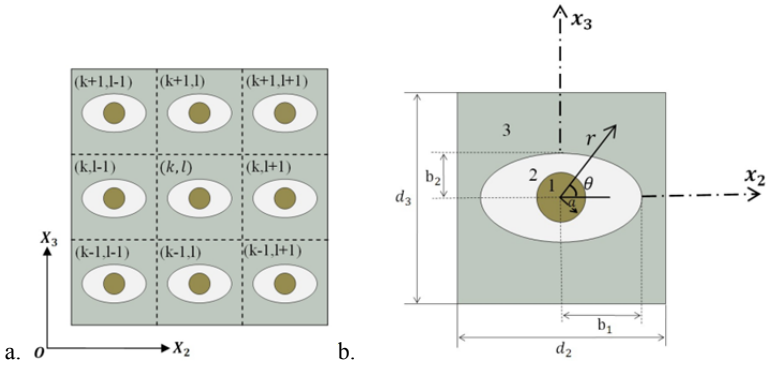

Fig. 1. (a) An anisotropic elastic metamaterial made of cylinders coated with elliptical soft layer in a matrix; (b) The(k,l) element (RVE).

2.1 A simplified model of the elastic metamaterial

For the elastic metamaterial with the complicated microstructure geometry shown in Fig.1, analytical-based homogenization approaches have difficulties to find the exact local scattering wave field. In this study, the RVE with the continuous microstructure is first simplified to the RVE with a discrete mass-spring microstructure with spring constants K_2 and K_3, as shown in Fig. 2 [30], based on the strain energy equivalence between the two systems. The inclusion core is reduced as a rigid mass $m_1 = \rho_1 \pi a^2$ and the coating material is replaced by the springs with the spring constants K_2 and K_3 because of the large stiffness mismatch between the core and the coating material. The spring constants K_2 and K_3 can be numerically determined as $K_\alpha = F_\alpha/\gamma_\alpha$ with $\alpha = 2,3$, where F_α is the restoring force on the outer fixed boundary of the coating layer and $u_\alpha = \gamma_\alpha$ is the applied displacement along x_2 and x_3 directions of the coating layer.

For the general geometry of the coating layer, the problem can be numerically solved by using finite element method (FEM).

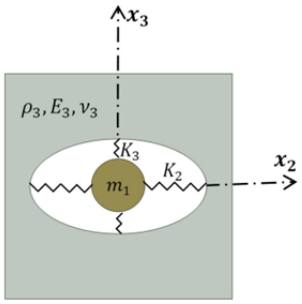

Fig. 2. The equivalent RVE for the (k,l) element of the elastic metamaterial.

2.2 A multi-displacement microstructure model

In this subsection, a new homogeneous high-order continuum theory will be proposed to homogenize the simplified elastic anisotropic metamaterial, as shown in Fig. 3. For the elastic metamaterial, the inner mass will move out-of-phase with respect to the motion of the composite when the frequency is close to the resonant frequency of the inner mass, which is called the dipolar motion. The schematic illustration of the dipolar motion in the elastic metamaterial near the resonant frequency is shown in Fig. 4.

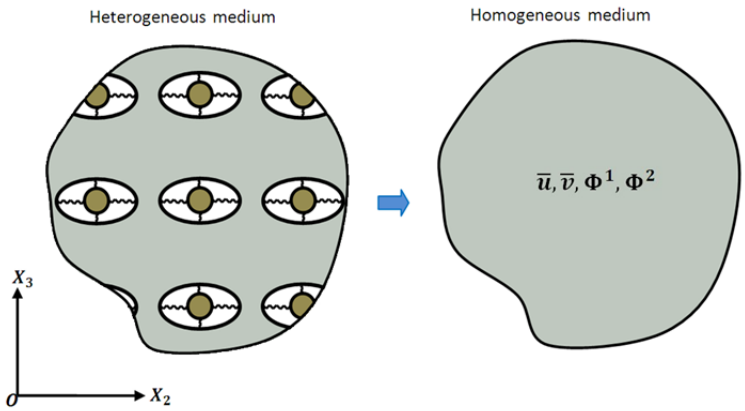

Fig.3. Heterogeneous medium replaced by a homogeneous medium.

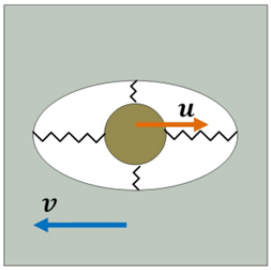

Fig.4. A schematic illustration of dipolar motion in the metamaterial near the resonant frequency.

The conventional continuum model cannot capture the dipolar motion, therefore, a continuum model with additional multi-displacement variables should be introduced. Specifically, attention is also paid to the problem with wavelengths in an order of the dimension of the unit-cell. To describe the relative high-frequency dynamic behaviors, microstructure kinetic variables are also needed. In the formulation, we assume the lead core is rigid because of its high modulus and the local displacements in the matrix can be approximated by linear series expansions in terms of quantities which are defined at the center of the element. The micro-deformations are assumed as follows:

(1) In the inclusion of the cell (k,l), $(r < a)$

$$\boldsymbol{u}^1 = \bar{\boldsymbol{u}} \tag{1a}$$

(2) In the matrix of the cell (k,l), $(r \geq \bar{b})$

$$\boldsymbol{u}^3 = \bar{\boldsymbol{v}} + \bar{b}\boldsymbol{\Phi}^{\boldsymbol{2}}\boldsymbol{\Theta} + \left(r - \bar{b}\right)\boldsymbol{\Phi}^{\boldsymbol{3}}\boldsymbol{\Theta} \tag{1b}$$

where

$$\boldsymbol{u}^1 = \left[u_2^{1(k,l)} \quad u_3^{1(k,l)}\right]^T, \bar{\boldsymbol{u}} = \left[\bar{u}_2^{(k,l)} \quad \bar{u}_3^{(k,l)}\right]^T,$$

$$\boldsymbol{u}^3 = \left[u_2^{3(k,l)} \quad u_3^{3(k,l)}\right]^T, \bar{\boldsymbol{v}} = \left[\bar{v}_2^{(k,l)} \quad \bar{v}_3^{(k,l)}\right]^T, \boldsymbol{\Theta} = [cos\theta \quad sin\theta]^T,$$

$$\boldsymbol{\Phi}^{\boldsymbol{2}} = \begin{bmatrix} \phi_{22}^{2(k,l)} & \phi_{32}^{2(k,l)} \\ \phi_{23}^{2(k,l)} & \phi_{33}^{2(k,l)} \end{bmatrix}, \boldsymbol{\Phi}^{\boldsymbol{3}} = \begin{bmatrix} \phi_{22}^{3(k,l)} & \phi_{32}^{3(k,l)} \\ \phi_{23}^{3(k,l)} & \phi_{33}^{3(k,l)} \end{bmatrix}, \bar{b} = \frac{b_1 b_2}{\sqrt{{b_1}^2 sin^2\theta + {b_2}^2 cos^2\theta}}.$$

where $\bar{\boldsymbol{u}}, \bar{\boldsymbol{v}}, \boldsymbol{\Phi}^{\boldsymbol{2}}, \boldsymbol{\Phi}^{\boldsymbol{3}}$ are global variables in functions of (X_2, X_3, t), the local displacements $\boldsymbol{u}^1$ and $\boldsymbol{u}^3$ are functions of (X_2, X_3, x_2, x_3, t), or in other words, functions of (X_2, X_3, r, θ, t). Physical interpretation of the terms in Eq. (4) is that global displacements $\bar{\boldsymbol{u}}$ and $\bar{\boldsymbol{v}}$ are the displacements of the center of the inclusion and the center of the matrix, respectively; while $\boldsymbol{\Phi}^{\boldsymbol{2}}$ represents micro-deformation in the area within the inner boundary of the matrix, and $\boldsymbol{\Phi}^{\boldsymbol{3}}$ represents micro-deformation in the matrix. It should be mentioned that the additional displacement components are necessary to capture the dipolar motion in the metamaterial, which is different from the microstructure continuum theory [39]. In the microstructure continuum theory, additional microstructure variables were only introduced to capture the micro-deformation in the microstructure.

In principle, the boundary condition between the unit-cell and the neighboring cells should be satisfied on every point of the boundaries. However, the approximated local field, assumed in Eq. (1b), cannot exactly satisfy the point-to-point continuity at the boundaries. In this study, relaxation boundary continuity conditions, which are defined as averaged displacement continuity conditions at the interfaces of the cells, are suggested as:

$$\int_{-d_2/2}^{d_2/2} \left[u_\alpha^{3(k+1,l)}|_{x_3=-\frac{d_3}{2}} - u_\alpha^{3(k,l)}|_{x_3=\frac{d_3}{2}} \right] dx_2 = 0 \tag{2a}$$

$$\int_{-d_3/2}^{d_3/2} \left[u_\alpha^{3(k,l+1)}|_{x_2=-\frac{d_2}{2}} - u_\alpha^{3(k,l)}|_{x_2=\frac{d_2}{2}} \right] dx_3 = 0 \tag{2b}$$

where $u_\alpha^{3(k+1,l)}$ and $u_\alpha^{3(k,l+1)}$ represent displacement components of the matrix in the cells $(k+1,l)$ and $(k,l+1)$. Eq. (2a) represents the averaged displacement continuity on the boundary between the cell (k,l) and the cell $(k+1,l)$; and Eq. (2b) represents the averaged displacement continuity on the boundary between the cell (k,l) and the cell

$(k, l+1)$. This approximate is more reasonable for relatively low frequency cases. Substituting the local displacement in the matrix Eq. (1b) into Eq. (2a) results in

$$\bar{v}_\alpha^{(k+1,l)} - \bar{v}_\alpha^{(k,l)} - \frac{b_1 d_3}{d_2} \ln\left(\frac{1+\sqrt{1+\xi^2}}{\xi}\right)\left(\phi_{3\alpha}^{2(k+1,l)} - \phi_{3\alpha}^{3(k+1,l)} + \phi_{3\alpha}^{2(k,l)} - \phi_{3\alpha}^{3(k,l)}\right) - \frac{d_3}{2}\left(\phi_{3\alpha}^{3(k+1,l)} + \phi_{3\alpha}^{3(k,l)}\right) = 0 \quad (3a)$$

where $\xi = \frac{b_1 d_3}{b_2 d_2}$.

Similarly, another continuous condition can be obtained from Eq. (5b) as

$$\bar{v}_\alpha^{(k,l+1)} - \bar{v}_\alpha^{(k,l)} - \frac{b_2 d_2}{d_3} \ln\left(\xi + \sqrt{1+\xi^2}\right)\left(\phi_{2\alpha}^{2(k,l+1)} - \phi_{2\alpha}^{3(k,l+1)} + \phi_{2\alpha}^{2(k,l)} - \phi_{2\alpha}^{3(k,l)}\right) - \frac{d_2}{2}\left(\phi_{2\alpha}^{3(k,l+1)} + \phi_{2\alpha}^{3(k,l)}\right) = 0 \quad (3b)$$

The corresponding local strain in the matrix can be obtained as

$$\boldsymbol{\varepsilon}^3 = \nabla \otimes \boldsymbol{u}^3 \quad (4)$$

where ∇ is the differentiation operator in the local coordinate system (x_2, x_3), $\boldsymbol{\varepsilon}^3 = \begin{bmatrix} \varepsilon_{22}^{3(k,l)} & \varepsilon_{23}^{3(k,l)} \\ \varepsilon_{32}^{3(k,l)} & \varepsilon_{33}^{3(k,l)} \end{bmatrix}$ is the strain tensor of the matrix.

Based on the displacement expressions in Eq. (1), the total kinetic energy density in the cell (k, l) can be calculated as

$$T_{ave}^{(k,l)} = \frac{1}{A_c}\left(T^{1(k,l)} + T^{3(k,l)}\right) \quad (5)$$

where $T^{1(k,l)}$ and $T^{3(k,l)}$ are the kinetic energies in the inclusion and matrix, respectively.
On the other hand, the strain deformation energy in the spring within the cell (k, l) can be obtained as
$W^{s(k,l)} =$

$$K_2\left[\left(\bar{v}_2^{(k,l)} - \bar{u}_2^{(k,l)}\right)^2 + \left(b_1 \phi_{22}^{2(k,l)}\right)^2 + \left(b_1 \phi_{32}^{2(k,l)}\right)^2\right] + K_3\left[\left(\bar{v}_3^{(k,l)} - \bar{u}_3^{(k,l)}\right)^2 + \left(b_2 \phi_{33}^{2(k,l)}\right)^2 + \left(b_2 \phi_{23}^{2(k,l)}\right)^2\right] \quad (6)$$

and the strain deformation energy in the matrix for the plane stress problem is

$$W^{m(k,l)} = \frac{E_3}{2(1-\nu_3{}^2)} \iint_{A_3} \left[\left(\varepsilon_{22}^{3(k,l)}\right)^2 + \left(\varepsilon_{33}^{3(k,l)}\right)^2 + 2\nu_3\left(\varepsilon_{22}^{3(k,l)}\right)\left(\varepsilon_{33}^{3(k,l)}\right) + 2(1-\nu_3)\left(\varepsilon_{23}^{3(k,l)}\right)^2\right] dA_3 \quad (7)$$

The total strain deformation energy averaged over the volume of cell (*k, l*) yields

$$W_{ave}^{(k,l)} = \frac{1}{A_c}\left(W^{s(k,l)} + W^{m(k,l)}\right) \quad (8)$$

To obtain a continuum model, we now introduce fields that are continuous in the global coordinate system X_2 and X_3, and the values at $X_2 = X_2^l$ and $X_3 = X_3^k$ coincide with those in the actual micro (local) field variables at the center of the cell. Therefore, we can consider the strain energy density $W(X_2, X_3, t)$ and the kinetic energy density $T(X_2, X_3, t)$ as continuous functions. Based on Eq. (5), the kinetic energy density $T(X_2, X_3, t)$ in the continuum field is

$$T(X_2, X_3, t) = T_{ave}^{(k,l)} = \frac{1}{A_c}\left(T^{1(k,l)} + T^{3(k,l)}\right) \quad (9)$$

and the strain energy density $W(X_2, X_3, t)$ is

$$W(X_2, X_3, t) = W_{ave}^{(k,l)} = \frac{1}{A_c}\left(W^{s(k,l)} + W^{m(k,l)}\right) \quad (10)$$

At the same time, the continuity conditions in Eq. (3) can be written in the terms of continuous variables by considering the field variables as continuous functions of X_2 and X_3, as

$$S_{3\alpha}(X_2,X_3,t)=\frac{\partial \bar{v}_\alpha}{\partial X_3}-\frac{2b_1}{d_2}\ln\left(\frac{1+\sqrt{1+\xi^2}}{\xi}\right)\left(\phi^2_{3\alpha}-\phi^3_{3\alpha}+\frac{d_3}{2}\frac{\partial\phi^2_{3\alpha}}{\partial X_3}-\frac{d_3}{2}\frac{\partial\phi^3_{3\alpha}}{\partial X_3}\right)-\phi^3_{3\alpha}-\frac{d_3}{2}\frac{\partial\phi^3_{3\alpha}}{\partial X_3}=0 \tag{11a}$$

$$S_{2\alpha}(X_2,X_3,t)=\frac{\partial \bar{v}_\alpha}{\partial X_2}-\frac{2b_2}{d_3}\ln\left(\xi+\sqrt{1+\xi^2}\right)\left(\phi^2_{2\alpha}-\phi^3_{2\alpha}+\frac{d_2}{2}\frac{\partial\phi^2_{2\alpha}}{\partial X_2}-\frac{d_2}{2}\frac{\partial\phi^3_{2\alpha}}{\partial X_2}\right)-\phi^3_{2\alpha}-\frac{d_2}{2}\frac{\partial\phi^3_{2\alpha}}{\partial X_2}=0 \tag{11b}$$

where $\alpha=2,3$.

Considering a fixed regular region V of the medium, the displacement equations of motion can be obtained by employing Hamilton's principle for independent variables in V and a specified time interval $t_0\le t\le t_1$as

$$\delta\int_{t_0}^{t_1}\int_V F dt dV+\int_{t_0}^{t_1}\delta W_1 dt=0 \tag{12}$$

where $F=T-W$, $\delta W_1$is the variation of the work done by external forces, and $dV$is the scalar volume element. For the current model, there are no existing external forces and the continuity conditions can be considered as subsidiary conditions through the use of Lagrangian multipliers, so the problem can be redefined as

$$\delta\int_{t_0}^{t_1}\int_V F dt dV=0 \tag{13}$$

With $F=T-W-\sum_{\alpha=2}^{3}(\Gamma_{2\alpha}S_{2\alpha}+\Gamma_{3\alpha}S_{3\alpha})$ (14)

where the Lagrangian multipliers $\Gamma_{2\alpha}$ and $\Gamma_{3\alpha}$are functions of X_2, X_3 and t. Since the function F as given in Eq. (14) depends only on the global field variables (X_2,X_3,t) and their first order derivatives, the system of the Euler equations can be written as

$$\sum_{r=1}^{3}\frac{\partial}{\partial p_r}\left[\frac{\partial F}{\partial\left(\frac{\partial f_s}{\partial p_r}\right)}\right]-\frac{\partial F}{\partial f_s}=0 \tag{15}$$

where $f_s(s=1,2,\ldots,16)$ represent the sixteen dependent variables $\bar{u}_\alpha$, $\bar{v}_\alpha$, $\phi^2_{2\alpha}$, $\phi^2_{3\alpha}$, $\phi^3_{2\alpha}$, $\phi^3_{3\alpha}$, $\Gamma_{2\alpha}$ and $\Gamma_{3\alpha}$ $(\alpha=2,3)$; and p_r $(r=1,2,3)$ are the spatial variables X_2, X_3 and time variable t. A system of sixteen governing equations of motion can be obtained from the Eq. (15).

2.3 Multi-displacement microstructure modeling for the chiral metamaterials

The chiral metamaterials are the periodical structure similar to the sketch shown in Fig.1, except that the springs are no longer vertical or horizontal, but inclined to form a chiral structure. The number of springs which inclined to connect the core and the matrix is N, which is an even number. And the elastic constant of the springs is K_s. The representative volume element (RVE) with $N=6$ springs are shown in Fig. 5.

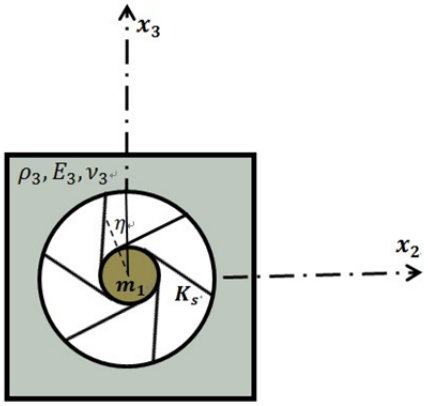

Fig. 5. The RVE for the (k,l) element of the chiral metamaterials.

Because of the additional displacement motion of the inner core, the additional rotation variable is needed. The micro-deformations are assumed as follows:

(3) In the inclusion of the cell (k,l), *(r<a)*

Displacement $\boldsymbol{u}^1 = \bar{\boldsymbol{u}}$

Rotation $\bar{\boldsymbol{\varphi}}$

(4) In the matrix of the cell (k,l), *(r≥ b)*

$$\boldsymbol{u}^3 = \bar{\boldsymbol{v}} + \bar{b}\boldsymbol{\Phi}^{\mathbf{2}}\boldsymbol{\Theta} + \left(r - \bar{b}\right)\boldsymbol{\Phi}^{\mathbf{3}}\boldsymbol{\Theta} \tag{16}$$

Where the global variable $\bar{\boldsymbol{\varphi}}$ indicates the rotation of the inner core and is in functions of (X_2, X_3, t).

the strain deformation energies in the springs can be obtained as

$$W^{s(k,l)} = \frac{1}{2}K_s \sum_{n=1}^{N}\Big\{C_1{}^2\left[\bar{v}_1^{(k,l)} + bC_2\phi_{11}^{1(k,l)} + bS_2\phi_{21}^{1(k,l)} - \bar{u}_1^{(k,l)} - aC_1\bar{\varphi}^{(k,l)}\right]^2 + \mathrm{S}_1{}^2\left[\bar{v}_2^{(k,l)} + bC_2\phi_{12}^{1(k,l)} + bS_2\phi_{22}^{1(k,l)} - \bar{u}_2^{(k,l)} - aS_1\bar{\varphi}^{(k,l)}\right]^2 + 2C_1\mathrm{S}_1\left[\bar{v}_1^{(k,l)} + bC_2\phi_{11}^{1(k,l)} + bsS_2\phi_{21}^{1(k,l)} - \bar{u}_1^{(k,l)} - aC_1\bar{\varphi}^{(k,l)}\right]\left[\bar{v}_2^{(k,l)} + bC_2\phi_{12}^{1(k,l)} + bS_2\phi_{22}^{1(k,l)} - \bar{u}_2^{(k,l)} - aS_1\bar{\varphi}^{(k,l)}\right]\Big\} \tag{17}$$

Where $\beta = \frac{\pi}{2} + \eta - \arccos(\frac{a}{b})$, N is the number of the springs. $C_1 = cos\left((n-1)\frac{2\pi}{N} + \eta\right)$, $\mathrm{S}_1 = sin\left((n-1)\frac{2\pi}{N} + \eta\right)$. $C_2 = cos\left((n-1)\frac{2\pi}{N} + \beta\right)$, $S_2 = sin\left((n-1)\frac{2\pi}{N} + \beta\right)$

Following the same procedure in section 2.2, the 17 governing equations with 17 variables can be obtained.

3. Modal Verification

To verify the proposed continuum model, let us first consider a two-dimensional elastic metamaterial with a cylinder heavy core coated with a circular soft layer and embedded in matrix in a square lattice array. The microstructure

geometry parameters are listed in Table 1 and the material parameters are provided in Table 2. Based on the simplified model for the continuous systems, spring constants for the 2D plane stress problem with the circle coated metamaterial can be numerically determined as $K_2 = K_3 = 1.184 \times 10^7 N/m$. It should be mentioned that for the current microstructure geometry, when the coating material is incompressible (the Poisson's ratio of the coat material ν_2 is about 0.5), the analytical solution for the spring constants [42] is also available as $K_2 = K_3 \cong \frac{40\pi\mu_2(a^2+b^2)}{25(a^2+b^2)\ln(b/a)-9(b^2-a^2)}$, where μ_2 is the shear modulus of the coating material $\mu_2 = \frac{E_2}{2(1+\nu_2)}$. The good agreement about the spring constant's prediction between the two methods shows the accuracy of the current numerical method.

Table 1. The microstructure geometry parameters.

Lattice parameters	Elliptical coat	Circle coat
$d_2 = d_3$	$20mm$	$20mm$
a	$3mm$	$5.155mm$
b_1	$7mm$	$7.14mm$
b_2	$5mm$	$7.14mm$

Table 2. The constituent material parameters.

The parameters	Core: lead	Coating: rubber	Matrix: epoxy
Mass density	ρ_1: $11.31 \times 10^3\ kg/m^3$	ρ_2: $0.92 \times 10^3\ kg/m^3$	ρ_3: $1.11 \times 10^3\ kg/m^3$
Young's modulus	E_1: $1.3 \times 10^{10}\ N/m^2$	E_2: $1.5 \times 10^6\ N/m^2$	E_3: $2.35 \times 10^9\ N/m^2$
Poisson's ratio	ν_1: 0.435	ν_2: 0.499	ν_3: 0.38
Area	A_1: πa^2	A_2: $\pi(b_1 b_2 - a^2)$	A_3: $d_2 d_3 - \pi b_1 b_2$

For a longitudinal wave propagation along X_2 direction in the metamaterial with infinite dimension in X_3 direction, the available kinematic variables include multi-displacement variables $\bar{u}_2, \bar{v}_2$, the microstructure field variables ϕ_{22}^2, ϕ_{22}^3 and the Lagrangian multiplier Γ_{22}. Therefore, five governing equations can be obtained. For the longitudinal wave propagating along X_2 direction, the continuum wave fields can be defined as

$$\{\bar{u}_2, \bar{v}_2, \phi_{22}^2, \phi_{22}^3, \Gamma_{22}\} = \{B_1, B_2, B_3, B_4, B_5\} \exp[i(q_2 X_2 - \omega t)] \quad (18)$$

where $i = \sqrt{-1}$,B_1,B_2, B_3, $B_4$and $B_5$are constant amplitudes, q_2 is the wave-number in X_2 direction, and ω is the angular frequency. For a nontrivial set of solutions the determinant of the coefficients must vanish to yield the dispersion relation. The exact wave dispersion curves can also be calculated by using commercial finite element (FE) software, ANSYS 12.0. In the FE model, Plane-82 element is used to model the elastic medium, and Combine-14 elements are used to model the springs. After properly applying boundary conditions for the model, modal analysis is conducted to obtain the natural frequencies, from which the dispersion curve can be obtained. Fig.6(a) shows comparison of the normalized dispersion curves of the longitudinal wave predicted by the current multi-displacement microstructure continuum model, the reduced single-displacement continuum model, and the FE simulation, where $\omega_{0L} = \sqrt{2K_2/m_1} = 5007.37\,{}^{rad}/_{s}$ and the resonant frequency is $f_{0L} = \omega_{0L}/(2\pi) = 797Hz$. The single-displacement model is reduced from the current model by removing the additional global displacement variable. It is found that the multi-displacement microstructure continuum model can give excellent prediction for acoustic wave mode and is also reasonably good for the optic wave mode for $q_2 d_2 < 0.9$. The band gap behavior of the elastic metamaterial can be accurately predicted by

using the current model, which is very useful for the design of the desirable elastic metamaterial. It is also very interesting to note that the band gap behavior cannot be captured when only single-displacement (conventional) continuum model is adopted. This is understandable because no additional degrees of freedom are used to capture the local dipolar resonance phenomenon. In addition, it is noticed that the current model has difficulty in capturing the optic wave mode when the frequency is around $\omega/\omega_{0L} = 8.48$ (f=6757Hz). Based on the eigenmode analysis at this frequency, it can be found that the resonance deformation is focus on the coating layer and no motions occur in the core and host matrix, which is similar to the quadrupolar resonance. To capture the quadrupolar resonance in the metamaterial, additional microstructure kinematic variables in the coating layer may be needed.

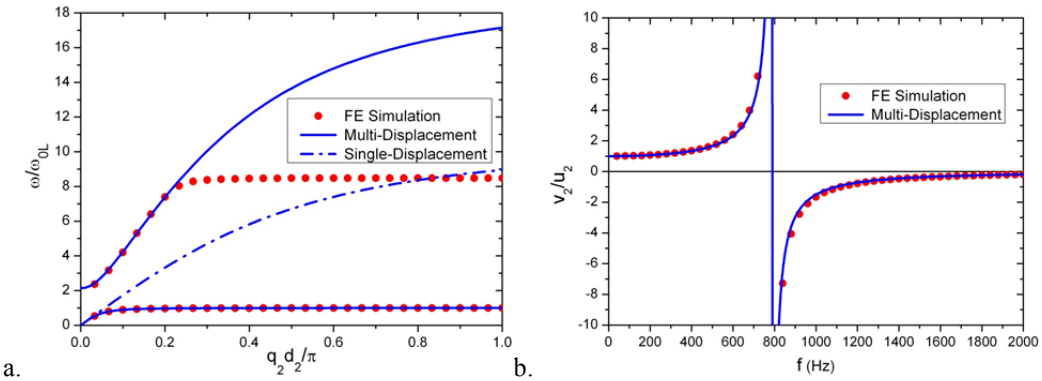

Fig.6. (a). Comparison of the normalized dispersion curves by the current model, the reduced single-displacement model and the FE simulation for longitudinal wave propagation. (b). The displacement amplitude ratio of the matrix to the core in function of the frequency.

Fig.6(b) shows the wave amplitude ratio of the matrix to the core in a function of the frequency predicted by the current model and the finite element method (FEM). The very good agreement between the current model and FEM is observed for the local displacement prediction in the elastic metamaterial, which is impossible for the conventional continuum models. Around $f = 797Hz$, there exists a resonance in the metamaterial in which the displacement of the core is very large and experiences a very sharp change from the in-phase state to the out-of-phase state. A large displacement ratio enhancement can be observed in the in-phase resonance region. From eigenmode analysis, we can find that the core inclusion moves opposite to the motion in the matrix in the band gap frequency range, which cannot be captured through the conventional continuum model.

4. Numerical Simulation and Discussions

4.1 Wave propagation in anisotropic elastic metamaterials

It is well known that for isotropic metamaterials, wave propagation behavior is identical for any wave propagation direction. For anisotropic elastic metamaterials, wave propagation behavior is different along different directions and is direction-dependent. Fig. 7(a) and (b) show the comparison of the normalized dispersion curves for the transverse shear wave propagation along X_2 and X_3 directions for the anisotropic elastic metamaterial, respectively. In the figures, the material properties are the same as in Table 2. The microstructure geometry parameters are shown in Table 1 with an

elliptical coating medium, from which the spring constants are numerically obtained as $K_2 = 4.93 \times 10^6 kg/m, K_3 = 6.45 \times 10^6 kg/m$. The resonant angular frequencies are $\omega_{0T2} = \sqrt{2K_3/m_1}$ and $\omega_{0T3} = \sqrt{2K_2/m_1}$, respectively. It is found that the current model can provide good prediction of dispersion curves for both the acoustic wave mode and the optic wave mode along different wave propagation directions. The anisotropic wave propagation behavior can be observed from the different wave dispersion curves along different directions. From the numerical simulation, it is also concluded that the band gap frequency regime is within the same frequency when the effective mass density becomes negative, which confirms wave mechanism in the current anisotropic metamaterial is caused by the dipolar wave motion.

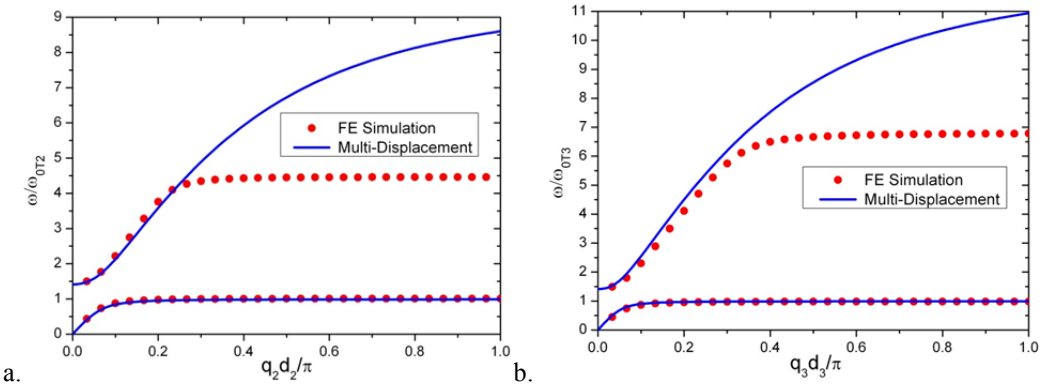

Fig.7. Comparison of the normalized dispersion curves for the anisotropic metamaterial for transverse wave propagation (a).along X_2direction; (b). along X_3direction.

4.2 Wave propagation in the chiral metamaterials

For the chiral metamaterial (the RVE sketch is shown in Fig.5), we consider the wave propagation similarly. The springs constant between the inclusion and the matrix are chosen as $K_s = 1 \times 10^8 N/m$, the number is $N = 6$, and the angle $\eta = 30°$.

For the harmonic wave propagation, the continuum wave fields can be defined as

$$f_s = B_s \exp[i(q_2 X_2 + q_3 X_3 - \omega t)] \quad (s = 1,2,\dots,17) \tag{19}$$

where $i = \sqrt{-1}$, B_s are constant amplitudes, q_2, q_3 are the wavenumbers, and ω is the angular frequency. Substitution of (19) into the equations of motion yields 17 homogeneous equations for B_s. For a nontrivial set of solutions the determinant of the coefficients must vanish to yield the dispersion relation. Fig.8 shows a comparison of the dispersion curves of the wave predicted by the current multi-displacement microstructure model and the finite element simulation (FE simulation) in the Irreducible Brillouin Zone. We can clearly see that the multi-displacement theory can capture the low-frequency dispersion. For the higher frequency, our current model is failed to capture the transverse because the rotation and the shear mode are uncoupled in our current model while they are coupled in real wave propagation (Ansys simulation). The most important feature of the dispersion curves is that there is an additional band (the 3rd band) which is neither longitudinal nor transverse. The existence of the rotation of the core can explain the additional 3rd band. Fig.9 shows the effective mass of the chiral metamaterial through the Ansys method, where $m_0 = m_1 + m_3 = \rho_1 \pi a^2 + \rho_3 (d_2 d_3 - \pi b^2)$ is the static mass of the unit-cell. The frequency range $f = 2\text{kHz}\sim7\text{kHz}$ is shown and the negative mass band if corresponding to the band gap of the dispersion curves shown in Fig.8.

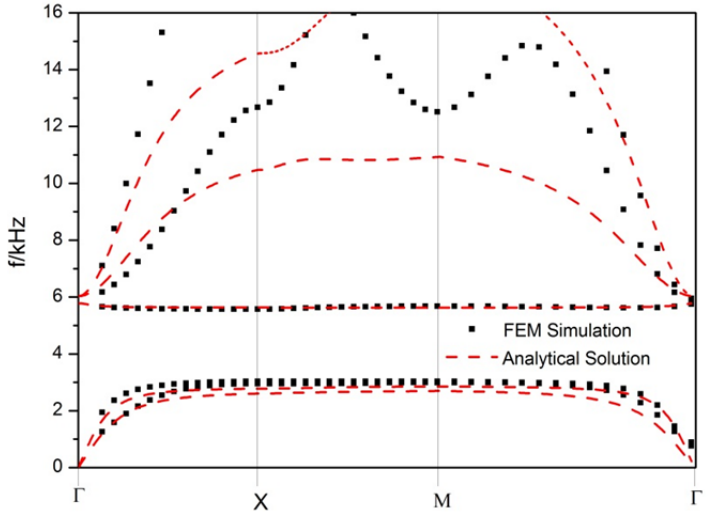

Fig.8. The dispersion curves in the first Brillouin Zone

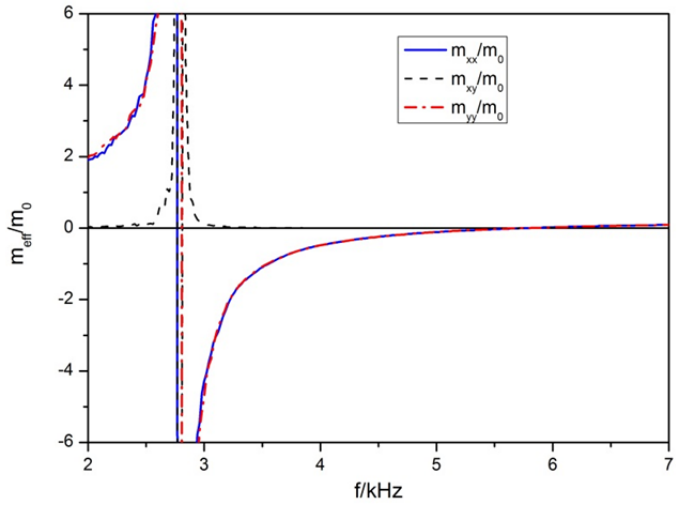

Fig.9. The effective mass of the chiral metamaterial

5. CONCLUSION

In this paper, an elastic metamaterial made of lead cylinders coated with elliptical rubbers in an epoxy matrix is considered. To describe global dynamic behavior in the elastic metamaterial, a new multi-displacement microstructure continuum model is developed to obtain the macroscopic governing equations of the anisotropic elastic metamaterial. Especially, one more variable is needed to describe the rotation of the core for the chiral metamaterial. The current model is verified through comparison of wave dispersion curves predicted by the current model and the finite element simulation. Very good agreement is observed in both the acoustic and optic wave modes. The proposed model may provide an efficient tool for modeling of the elastic metamaterial with complex microstructures.

ACKNOWLEDGEMENT

This work was supported by the NASA Arkansas EPSCoR RID program.

REFERENCE

[1] X. Hu, C. T. Chan and J. Zi, Two-dimensional sonic crystals with Helmholtz resonators, Phys. Rev. E 71 (2005) 055601(R).

[2] X. Hu and C. T. Chan, Refraction of water waves by periodic cylinder arrays, Phys. Rev. Lett. 95 (2005) 154501.

[3] Z. Liu, X. Zhang, Y. Mao, Y. Y. Zhu, Z. Yang, C. T. Chan and P. Sheng, Locally resonant sonic materials, Science 289 (2000) 1734-1736.

[4] S. Yang, J. H. Page, Z. Liu, M. L. Cowan, C. T. Chan and P. Sheng, Ultrasound tunneling through 3D phononic crystals, Phys. Rev. Lett. 88 (2002) 104301.

[5] Z. Hou, X. Fu and Y. Liu, Calculational method to study the transmission properties of phononic crystals, Phys. Rev. B 70 (2004) 014304.

[6] N. Fang, D. Xi, J. Xu, M. Ambati, W. Srituravanich, C. Sun and X. Zhang, Ultrasonic metamaterials with negative modulus, Nat. Mater. 5 (2006) 452-456.

[7] S. Gonella, A. C. To and W. K. Liu, Interplay between phononic bandgaps and piezoelectric microstructures for energy harvesting, J. Mech. Phys. Solids 57 (2009) 621-633.

[8] X. N. Liu, G. K. Hu, G. L. Huang and C. T. Sun, Wave propagation characterization and design of two-dimensional elastic chiral metacomposite, J. Vib. Acoust. 330 (2011)

[9] M. Kafesaki and E. N. Economou, Multiple scattering theory for 3D periodic acoustic composites , Phys. Rev. B 60 (1999) 11993.

[10] X. Hu, K. M. Ho, C. T. Chan and J. Zi, Homogenization of acoustic metamaterials of Helmholtz resonators in fluid, Phys. Rev. B 77 (2008) 172301.

[11] P. Sheng, Introduction to wave scattering, localization, and mesoscopic phenomena, Academic, San Diego 1995.

[12] Z. Liu, C.T. Chan and P. Sheng, Analytic model of phononic crystals with local resonances, Phys. Rev. B 71 (2005) 014103.

[13] J. Mei, Z. Liu, W. Wen and P. Sheng, Effective mass density of fluid-solid composites, Phys. Rev. Lett. 96 (2006) 024301.

[14] Y. Wu, Y. Lai and Z. Q. Zhang, Effective medium theory for elastic metamaterials in two dimensions, Phys. Rev. B 76 (2007) 205313.

[15] Z. Yang, J. Mei, M. Yang, N. H. Chan and P. Sheng, Membrane-type acoustic metamaterial with negative dynamic mass, Phys. Rev. Lett. 101 (2008) 204301.

[16] X. M. Zhou and G. K. Hu, Analytic model of elastic metamaterials with local resonances, Phys. Rev. B 79 (2009) 195109.

[17] Y. Ding, Z. Liu, C. Qiu and J. Shi, Metamaterial with simultaneously negative bulk modulus and mass density, Phys. Rev. Lett. 99 (2007) 093904.

[18] M. G. Imhof, Multiple multipole expansions for elastic scattering, J. Acoust. Soc. Am. 100 (1996) 2969-2979.

[19] G. Wang, X. Wen, J. Wen, L. Shao and Y. Liu, Two-dimensional locally resonant phononic crystals with binary structures, Phys. Rev. Lett. 93 (2004) 154302.

[20] A. Khelif, P. A. Deymier, B. Djafari-Rouhani, J. O. Vasseur and L. Dobrzynski, Two-dimensional phononic crystal with tunable narrow pass band: Application to a waveguide with selective frequency, J. Appl. Phys. 94 (2003) 1308.
[21] D. Torrent and J. Sánchez-Dehesa, Anisotropic mass density by two-dimensional acoustic metamaterials, New J. Phys. 10 (2008) 023004.
[22] X. Ao and C. T. Chan, Far-field image magnification for acoustic waves using anisotropic acoustic metamaterials, Phys. Rev. E 77 (2008) 025601.
[23] J. R. Willis, Exact effective relations for dynamics of a laminated body, Mech. of Mater. 41 (2009) 385-393.
[24] J. R. Willis, Effective constitutive relations for waves in composites and metamaterials, Proc. R. Soc. A 2011 (doi:10.1098/rspa.2010.0620).
[25] A. L. Shuvalov, A. A. Kutsenko, A. N. Norris and O. Poncelet, Effective Willis constitutive equations for periodically stratified anisotropic elastic media, Proc. R. Soc. A 467 (2011) 1749-1769.
[26] S. Nemat-Nasser, J. R. Willis, A. Srivastava and A. V. Amirkhizi, Homogenization of periodic elastic composites and locally resonant sonic materials, Phys. Rev. B 83 (2011) 104103.
[27] M. Hirsekorn and P. P. Delsanto, Elastic wave propagation in locally resonant sonic material: Comparison between local interaction simulation approach and modal analysis, J. Appl. Phys. 99 (2006) 124912.
[28] Y. Gu, X. Luo and H. Ma, Low frequency elastic wave propagation in two dimensional locally resonant phononic crystal with asymmetric resonator, J. Appl. Phys. 105 (2009) 044903.
[29] Cz. Wozniak, Refined macro-dynamics of periodic structures, Arch. Mech. 45 (1993) 295-304.
[30] G. W. Milton and J. R. Willis, On modifications of Newton's second law and linear continuum elastodynamics, Proc. R. Soc. A 463 (2007) 855-880.
[31] G. W. Milton, New metamaterials with macroscopic behavior outside that of continuum elastodynamics, New J. Phys. 9 (2007) 359.
[32] J. J. Alibert, P. Seppecher and F. Dell'Isola, Truss modular beams with deformation energy depending on higher displacement gradients, Math. Mech. Solid. 8 (2003) 51-73.
[33] E. Cosserat and F. Cosserat, Théorie des corps déformables, A. Hermann et Fils, Paris, 1909.
[34] A. C. Eringen and E. S. Suhubi, Nonlinear theory of simple micro-elastic solids – I, Int. J. Engng. Sci. 2 (1964) 189-203.
[35] R. A. Toupin, Elastic materials with couple-stresses, Arch. Ration. Mech. Anal. 11 (1962) 385-414.
[36] A. C. Eringen, Microcontinuum field theories I: foundations and solids, Springer-Verlag, New York, 1999.
[37] R. D. Mindlin, Micro-structure in linear elasticity, Arch. Ration. Mech. Anal. 16 (1964) 51-78.
[38] C. T. Sun, J. D. Achenbach and G. Herrmann, Continuum theory for a laminated medium, J. Appl. Mech. 53 (1968) 467-475.
[39] G. L. Huang and C. T. Sun, Continuum modeling of solids with micro/nanostructures, Philos. Mag. 87 (2007) 3689-3707.
[40] R. Zhu, H. H. Huang, G. L. Huang and C. T. Sun, Microstructure continuum modeling of an elastic metamaterial, Int. J. Engng. Sci. 49 (2011) 1477-1485.
[41] A.P. Liu, R. Zhu, X.N. Liu, G.K.Hu and G.L. Huang, Multi-displacement microstructure continuum modeling of anisotropic elastic metamaterials, Wave Motion, in press.
[42] J. R. Barber, Elasticity, Springer, Dordrecht, 3rd Edition, 2010.